Melting behavior of $(Th,U)O_2$ and $(Th,Pu)O_2$ mixed oxides

P.S. Ghosh[a], N. Kuganathan[b], C.O.T Galvin[b], A. Arya[a], G.K. Dey[a], B.K. Dutta[c] and R.W. Grimes[b]

[a]Material Science Division, Bhabha Atomic Research Centre, Trombay, Mumbai 400 085, India

[b]Department of Materials, Faculty of Engineering, Imperial College, London, SW7 2AZ, UK

[c]Human Resource Development Division, Bhabha Atomic Research Centre, Trombay, Mumbai 400085, India

Abstract

The melting behaviors of pure ThO_2, UO_2 and PuO_2 as well as $(Th,U)O_2$ and $(Th,Pu)O_2$ mixed oxides (MOX) have been studied using molecular dynamics (MD) simulations. The MD calculated melting temperatures (MT) of ThO_2, UO_2 and PuO_2 using two-phase simulations, lie between 3650-3675 K, 3050-3075 K and 2800-2825 K, respectively, which match well with experiments. Variation of enthalpy increments and density with temperature, for solid and liquid phases of ThO_2, PuO_2 as well as the ThO_2 rich part of $(Th,U)O_2$ and $(Th,Pu)O_2$ MOX are also reported. The MD calculated MT of $(Th,U)O_2$ and $(Th,Pu)O_2$ MOX show good agreement with the ideal solidus line in the high thoria section of the phase diagram, and evidence for a minima is identified around 5 atom% of ThO_2 in the phase diagram of $(Th,Pu)O_2$ MOX.

1. Introduction

Investigations of thorium (^{232}Th) as a fuel for nuclear power reactors started in parallel with the corresponding first studies of uranium and plutonium. Thorium seemed an attractive prospect mainly due to its abundance, the opportunity to reduce the need for enrichment in the fuel cycle, the high conversion ratios (to ^{233}U) achievable in a thermal neutron spectrum, but also due to other neutron and thermal physical properties studied at this early stage of the nuclear power program. Despite this rather long list of advantages and fast depletion of uranium resources, thorium is not yet challenging the use of uranium fuel on a commercial basis, although research efforts regarding the thorium fuel cycle (ThFC) continue [1-3]. ^{232}Th is fertile, and by absorbing slow neutrons in the reactor environment it can transmute to ^{233}U [1-2], which is fissile. Therefore, ^{232}Th based fuels need a fissile material as a

'driver' (such as ^{235}U or ^{239}Pu) to facilitate a nuclear chain reaction. Thus, ^{232}Th based mixed oxides (MOX) ($(Th,U)O_2$ and $(Th,Pu)O_2$) are considered as a potential fuel for various reactor systems (*viz.*, conventional pressurized water reactors (PWR), advanced heavy water reactors (AHWR) and thermal breeder reactors) [1-3]. It has already been established that $(Th,Pu)O_2$ MOX fuel can be used in PWRs without any significant change in the reactor design [1,2]. Nevertheless, since it has not been widely used, a number of properties that are available to designers and regulators of UO_2 based fuels are not so well established for ThO_2 based fuels.

In view of the above, the melting behaviour of actinide oxides and their MOX is a fundamental property of a nuclear material related to its thermodynamical and structural stability. The melting temperature is also an important engineering parameter for nuclear fuel design and safety assessment, as it defines operational limits of nuclear fuel (for both UO_2 and ThO_2 based) in its application environment [1-3]. The onset of melting at the centerline of the fuel rod has been widely accepted as an upper limit to the allowable thermal rating of a nuclear fuel element [1,2]. The melting point (MP) must be taken into account when designing a new fuel, as it limits the power that can be extracted from the fuel element. Knowledge of the melting point is also important for the fabrication of chemically homogeneous fuel pellets of MOX (such as $(Th,U)O_2$ and $(Th,Pu)O_2$) since ThO_2 and UO_2 have high melting points of 3663 K and 3100 K, respectively, and relatively low diffusion coefficients at normal sintering temperatures [3]. Thorium dioxide exists up to its melting point as a single cubic fluorite phase, isomorphous, and completely miscible with UO_2 and PuO_2. Moreover, the melting points of the nuclear fuels are depreciated by factors such as; stoichiometry and composition, irradiation dose, impurities and their concentrations.

In order to understand the thermo-physical behavior of thoria based MOX fuels under reactor operation conditions, subject to irradiation, and to predict their performance under accident conditions, thermodynamic quantities such as, melting temperatures, enthalpy and densities of those solids as well as their liquid phases need to be evaluated. Moreover, determination of these thermodynamic properties for $(Th,Pu)O_2$ MOX by experiment is very difficult due to the radioactivity and toxicity of PuO_2 based systems, which require extensive and expensive safety precautions [1-3]. As a result, the number of studies addressing these thermodynamic quantities for PuO_2 and $(Th,Pu)O_2$ MOX is small. During the last four decades, even though melting temperatures of ThO_2 [6-10], UO_2 [11-20] as well as high temperature thermodynamic quantities of their MOX [21-33] have been widely investigated by various experimental techniques, melting behaviors of PuO_2, $(Th,U)O_2$ and $(Th,Pu)O_2$ MOX are much less in

evidence. Important thermodynamic quantities such as density and enthalpy increment of both solid and liquid phases as well as heat of fusion are only available for pure UO_2 [25,27,28]. For ThO_2, these thermodynamic quantities for the solid phase are available only over a limited temperature range [21-24, 26] and no data is available for the liquid phase. Recently, Böhler *et al.* [18] and Bruycker *et al.* [20] determined melting temperatures of PuO_2 using a laser heating method and pyrometry. Valu *et al.* [34] determined enthalpy increments of $Th_{1-x}Pu_xO_2$ (for x = 0, 0.03, 0.08, 0.30, 0.54, 0.85 and 1) using drop calorimetry in the temperature range 476 K to 1790 K. Still, high temperature enthalpy and density values of solid PuO_2, $(Th,Pu)O_2$ and$(Th,U)O_2$ MOX as well as their respective liquid phases are not available.

In this study, we employ classical molecular dynamics (MD) to calculate melting temperature as well as enthalpy increments and density for solid and liquid ThO_2, UO_2 and PuO_2. These MD calculated values are compared with available experimental values to assess the simulation methodology and the reliability of the interatomic potentials. Finally, melting temperatures and thermodynamic values of both solid and liquid phases of Th rich $(Th,U)O_2$ and $(Th,Pu)O_2$ MOX are determined, which are of importance for AHWR fuel applications [1-3].

2. Methodology

2.1 Empirical potential

The most recent empirical potential form for ThO_2, UO_2 [35] and PuO_2 [36] as well as their MOX [37] which is employed in this study, combines a pair-wise with a many body interaction term. The potential energy, E_i , of an atom i with respect to all other atoms can be represented as:

$$E_i = \frac{1}{2}\sum_j \varphi_{\alpha\beta}(r_{ij}) - G_\alpha\left(\sum_j \sigma_\beta(r_{ij})\right)^{\frac{1}{2}} \quad (1)$$

The pair interaction potential of two particles i and j of species α and β, separated by r_{ij} consists of a long-range Coulomb interaction ($\varphi_C(r_{ij})$) and a short range interaction. The short range interactions are developed by combining Morse and Buckingham forms ($\varphi^M(r_{ij})$ and $\varphi^B(r_{ij})$, respectively). Therefore,

$$\phi_{\alpha\beta}(r) = \phi_{\alpha\beta}^{(C)}(r) + \phi_{\alpha\beta}^{(B)}(r) + \phi_{\alpha\beta}^{(M)}(r) \quad (2)$$

$$\phi_{\alpha\beta}^{(C)}(r) = q_\alpha q_\beta / 4\pi\epsilon_0 r \quad (3)$$

$$\phi_{\alpha\beta}^{(B)}(r) = A_{\alpha\beta}\exp\left(-r/\rho_{\alpha\beta}\right) - C_{\alpha\beta}/r^6 \quad (4)$$

$$\phi_{\alpha\beta}^{(M)}(r) = D_{\alpha\beta}\left[\exp\left(-\beta_{\alpha\beta}\left(r - r'_{\alpha\beta}\right)\right) - 1\right]^2 \quad (5)$$

where $A_{\alpha\beta}$, $\rho_{\alpha\beta}$, $C_{\alpha\beta}$, $D_{\alpha\beta}$, $\beta_{\alpha\beta}$ *and* $r'_{\alpha\beta}$ are empirical parameters to describe Buckingham and Morse interactions between atoms *i* and *j*. For the Coulombic contribution, an effective ionicity, Z_α^{eff} is introduced to replace the formal charges of the ions with charges, $q_\alpha = Z_\alpha^{eff} e$; Z_α^{eff} = 2.2208 for tetravalent cations and $Z_\alpha^{eff} = -1.1104$ for oxygen anions.

The many body part of Equation (1) is achieved by a combination of a set of pairwise interactions ($\sum_j \sigma_\beta(r_{ij})$) between atom *i* and its nearest atoms and then passing it through a non-linear embedding function (the square root in equation (1)). Equation (6) gives the functional form of $\sigma_\beta(r_{ij})$ (n_β is the constant of proportionality) and the many-body energy term is proportional to $\sum_j \sigma_\beta^{1/2}(r_{ij})$ with G_α being the constant of proportionality in Equation (1).

$$\sigma_\beta(r_{ij}) = \frac{n_\beta}{r_{ij}^8} \quad (6)$$

An error function with a 1.5 Å cut-off distance is also added to Equation (6) in order to prevent dominance of non-physical forces arising from the many-body term over the short-range repulsive terms in the MD simulations. The upper limit cut-off distance for the interactions described in equations (4), (5) and (6) was set at 11.0 Å. Further details of the potential parameters have been published previously [35-37].

2.2 Solid solutions configuration

The most common methodology used to generate $(A,B)O_2$ MOX supercells, for MD simulations, is the random substitution of B atoms in A atom lattice sites by conserving intended average composition. The random distribution of substituted B ions in AO_2 depends on the configurational space available in the input structure and thus on the size of the simulation supercell. Different strategies for the random distribution of B atoms in the AO_2 supercells (keeping the average composition intact) access available configurational space differently [4,5]. In our study, thermo-physical quantities of $Th_{1-x}Pu_xO_2$ MOX are calculated over several randomly generated solid-solution configurations and averages of the calculated thermo-physical quantity over those individual configurations are reported.

Special quasirandom structures (*SQS*) is an alternative way to establish solid solution

configurations [38,39]. In *SQS*, the randomness is introduced by mimicking, as closely as possible, the most relevant, nearest neighbor pair and multisite correlation functions ($\Pi_{k,m}$, k = vertices and m = span of maximum nearest neighbor distances) of an infinite random solid solution within a finite supercell. In the present study, the determination of melting temperatures, enthalpy and density of $Th_{1-x}U_xO_2$ MOX was performed using a 96 atom *SQS* supercell generated from a face centered cubic *SQS* [40,41]. In **Table 1** all the pair and multisite correlation function values are compared with those of ideal solid solutions. It is also important to note that for the compositions (x) > 8/16 nearest neighbor pair and multisite correlation functions are similar to their x < 8/16 counterparts.

2.3 MD simulation for the determination of thermodynamic quantities

MD simulations for thermodynamic quantities were carried out using the MD code LAMMPS [42]. The Coulombic interactions were calculated using the Ewald method [43]. In the present study, the MD supercell was constructed having 4000 cations and 8000 anions by an array of 10x10x10 unit cells for $(Th,U)O_2$, $(Th,Pu)O_2$ MOX and their end members. To employ *SQS* methodology, a 96 atom *SQS* unitcell was constructured for $(Th,U)O_2$ MOX over the composition range and a 5x5x5 supercell of the *SQS* unitcell (4000 cations and 8000 anions) was used for MD simulations. MD runs were performed with a 2 fs time step in suitable temperature intervals over the temperature range 300 K to 6000 K, with the NPT ensemble at zero external pressure using the Berendsen barostat with a time constant of 0.5 ps and Nosé-Hoover thermostat with a time constant of 0.1 ps. Each simulation of thermodynamical quantities was carried out initially for 40 ps for equilibration (at the desired temperature) and then for another 10 ps to get average values of the thermodynamic quantities while heating the system.

To determine thermodynamic quantities for the liquid phase, a supercell containing 12000 atoms was first heated to 6000 K, to melt the system mechanically. Then the melted system was quenched to 2000 K from 6000 K in intervals of 100 K. At each temperature the system was equilibrated for 40 ps in the NPT ensemble at zero external pressure using the Berendsen barostat with a time constant of 0.5 ps and Nosé-Hoover thermostat with a time constant of 0.1 ps. The thermodynamical quantities were obtained from the average over the 10 ps run at each temperature.

2.4 Two-phase simulations for the determination of the melting temperatures

We performed two-phase simulations (TPS) in the isothermal-isobaric (NPT) ensemble to

determine the melting temperatures of ThO_2, UO_2, PuO_2 and $(Th,U)O_2$, $(Th,Pu)O_2$ MOX. A supercell of 36x6x6 unitcells (15552 atoms) containing both solid and liquid phases of pure ThO_2 was thermalized at T_1= 3000 K and P= 0 GPa via MD runs in the NPT ensemble. Next, atoms in one half of the simulation box (18x6x6 supercell) were kept fixed in their positions and MD runs were performed for the other half of the simulation box in the NPT ensemble at a sufficiently high temperature (T_2= 5000 K and P= 0 GPa) to create a liquid phase. The resulting supercell was then subjected to MD runs in the NPT ensemble at T_3= 4000 K (which is higher than the expected melting temperature) and P= 0 GPa, keeping the same half of the atoms fixed. The result of this process was a supercell containing solid ThO_2 at 3000 K in one half, and liquid ThO_2 at 4000 K in the other half. This ensures a minimum difference of stress between atoms in liquid and solid phases of the supercell [44]. This supercell was then used in the simulations of solidification and melting of ThO_2. The same methodology was adopted for UO_2 and PuO_2 but with T_1= 2500 K, T_2= 5000 K and T_3 = 3500 K. In order to determine the melting temperature of $(Th,U)O_2$ MOX, *SQS* generated structures were employed with T_1 = 2500 K, T_2 = 5000 K and T_3 = 4000 K. Similarly, for $(Th, Pu)O_2$ MOX, random solid-solution structures were employed with T_1 = 2500 K, T_2 = 5000 K and T_3 = 4000 K.

For the two-phase calculations a timestep of 2 fs and a Nosé-Hoover thermostat and barostat were applied in the constant pressure temperature (NPT) ensemble, using relaxation times of 0.1 ps and 0.5 ps, respectively. Thus, in this study, the MOX solid and liquid compositions are identical and differ from the slightly different composition that would exist in thermodynamic equilibrium.

3. Results

3.1 Melting temperatures of ThO_2, UO_2 and PuO_2

The two-phase supercell (as described in section 2.3) was heated in the NPT ensemble, where the temperature was increased from T_1 to T_3 in 100 K intervals. Each system ran for 1.6 ns of simulation time at a time step of 2 fs. For pure ThO_2, at 3600 K the solid phase of the simulation box progressed to occupy the entire box. In comparison, at 3700 K the liquid phase of the simulation box progressed to occupy the entire box. Next, the initial two-phase simulation box was heated from 3600 K to 3700 K in 25 K intervals. Each system was equilibrated for at least 2 ns. If the final state appeared to have both liquid and solid phases, more MD runs were performed until the final state of the supercell contained only one phase. Certain systems required as much as 4 ns of MD runs to arrive at a single phase. The transformation of the two-phase simulation box to a one-phase simulation box near the

predicted melting temperature is presented in **Figure 1**. A similar methodology was adopted for melting temperature calculations of pure UO_2 and PuO_2. The MD calculated range of temperatures where the phase change occurs for ThO_2, UO_2 and PuO_2 are 3650-3675 K, 3050-3075 K and 2800-2825 K, respectively.

3.2 Enthalpy and density variation of ThO_2, UO_2 and PuO_2

Figure 2(a) compares the MD calculated change in enthalpy (H(T)-H(300 K)) of ideal ThO_2 upon heating in the 300-6000 K range (*i.e.* for both solid and liquid phases) and cooling in the 6000-2000 K range, with experimentally available data [21-24]. Throughout the 300-3500 K temperature range the change in enthalpy matches well with experimental values, except with those of Hoch *et al.* [21]. **Figure 2(b)** shows our MD calculated density of ThO_2 in the 300-6000 K temperature range. The MD calculated values agree well with the experimental values reported by Momin *et al.* [26] in the 298-2273 K range. No experimental data are available for liquid thorium dioxide. MD calculated change in enthalpy (H(T)-H(300)) data is fitted to a functional form:

$$H(T)-H(300)=C_1\theta\left[\left(e^{\theta/T}-1\right)^{-1}-\left(e^{\theta/300}-1\right)^{-1}\right]+C_2\left[T^2-(300)^2\right]+C_3 e^{\beta/T} \quad (7)$$

in the 300-3600 K temperature range, where C_1 = 99.391, θ = 637.205, C_2 = -8.129 × 10^{-3}, C_3 = *3.35847* × 10^6, β = *12228.3*, T is the temperature in K, the enthalpy increment, H(T)-H(300), is in J mol^{-1} and $R^2 < 0.99$. Similarly, for the temperature range 3675-6000 K, MD calculated data of *H(l,T) – H(s,300)* for liquid ThO_2, in J mol^{-1}, is fitted to equation:

$$H(l,T)-H(s,300)=C_1+C_2T+C_3/T \quad (8)$$

where C_1 = 4.24348 × 10^4, C_2 =100.961 and C_3 = 9.8998 × 10^7. A similar set of equations were previously used to represent enthalpy increments of UO_2 for solid and liquid phases by Fink *et al.* [28]. The MD calculated density data for solid ThO_2 is fitted to a 3rd order polynomial equation in the 300-3600 K temperature range:

$$\rho(T)=C_1+C_2T+C_3T^2+C_4T^3 \quad (9)$$

to yield parameters C_1 = 10.084, C_2 = -2.4687 × 10^{-4}, C_3 = -9.10318 × 10^{-9} and C_4 = -8.4684 × 10^{-12}, where T is the temperature in K, the density is in g/cm^3 and $R^2 < 0.99$. Similarly, the MD calculated density of liquid ThO_2 is fitted to a linear equation in the temperature range 3675-6000 K of the form:

$$\rho(T)=C_1+C_2(T-3675) \quad (10)$$

where C_1 = 7.72082 and C_2 = -7.45616 × 10^{-4}.

Figure 3(a) shows the MD calculated change in enthalpy (H(T)-H(300 K)) of defect-free UO_2 upon heating in the 300-4500 K range, with the reported experimental data by Fink *et al.* [27-28] for both the solid and liquid phases. MD calculated density values for solid and liquid UO_2 are compared with experimental values in **Figure 3(b)**. MD calculated values for both solid and liquid phases are in good agreement with experimental values reported by Fink *et al.* [28]. Previously, Qin *et al.* [47] also calculated enthalpy increment and density as a function of temperature (300-5000 K range) for UO_2 and our MD calculated values are in complete agreement with their MD calculated results.

Figure 4(a) compares the MD calculated change in enthalpy (H(T)-H(300 K)) of ideal PuO_2 upon heating in the 300-6000 K range (*i.e.* for both solid and liquid phases) and cooling in the 6000-2000 K range, with experimentally reported values by Valu *et al.* [34]. Below 1000 K, MD calculated values of the change in enthalpy match well with experimental values but underestimate experimental values above 1000 K. **Figure 4(b)** shows our MD calculated density of PuO_2 in the 300-6000 K temperature range during heating and cooling, though no experimental data are available for solid and liquid plutonium dioxide. No data for the heat capacity or enthalpy of liquid PuO_2 are known, except a single enthalpy measurement by Ogard *et al.* [29].

This MD calculated change in enthalpy (H(T)-H(300)) data is fitted to a functional form (equation 7) in the 300-2800 K temperature range, where C_1 = 238.77, θ = 1269.05, C_2 = -68.9664×10^{-3}, C_3 = 5.42283×10^{6}, β = 8740.69, T is the temperature in K, the enthalpy increment, H(T)-H(300), is in J mol^{-1} and $R^2 < 0.99$. Similarly, for the temperature range 2825-6000 K, MD calculated data of *H(l,T) – H(s,300)* for liquid PuO_2, in J mol^{-1}, is fitted to equation (8) where $C_1 = 3.08813 \times 10^4$, C_2 = 96.033, $C_3 = 7.6837 \times 10^7$. The MD calculated density data for solid PuO_2 is fitted to a 3rd order polynomial (equation 9) in the 300-2800 K temperature range with C_1 = 11.7581, $C_2 = -3.229 \times 10^{-4}$, $C_3 = -1.0469 \times 10^{-8}$, $C_4 = -1.6744 \times 10^{-11}$, T is the temperature in K, the density is in g/cm^3 and $R^2 < 0.99$. Similarly, the MD calculated density of liquid ThO_2 is fitted to a linear equation (10) in the temperature range 2825-6000 K where C_1 = 8.4241 and $C_2 = -7.2256 \times 10^{-4}$.

At this point it is important to note, the potential set used in this study for ThO_2, UO_2 and PuO_2 efficiently reproduces experimentally reported elastic constants [36] and thermal properties [5,6,36,40,41]. Therefore, incorporation of many-body effects by EAM in conjunction with Buckingham and Morse pair-wise interaction the potential function, not only predict mechanical and low temperature thermal properties efficiently, but also predict melting temperatures with appreciable accuracy. So it is worth to explore melting behavior of MOX using this potential set.

3.3 Melting temperatures of $(Th,U)O_2$ MOX

Figure 5 shows the solidus and liquidus lines over the full composition range of ThO_2-UO_2 MOX calculated using **Equation 15**. Our MD calculated melting temperatures are also compared with previous experimental investigations by Latta *et al.* [30] and Böhler *et al.* [32]. These calculated melting temperatures are in very good agreement for the ThO_2 rich part of the phase diagram compared to the ideal solidus line calculated using **Equation 15** and experimentally determined values by Böhler *et al.* [32]. In the UO_2 rich part, the MD calculated values slightly underestimate the ideal solidus line but the estimated values are within the error bars of experimental measurements by Böhler *et al.* [32] (except at the 60 % composition). Our calculations suggest that the melting temperatures of UO_2 and UO_2-6.25 atom% ThO_2 are the same, which lie between 3050 K and 3075 K. This result is in agreement with the previous experimentally determined melting temperature where a minimum in the phase diagram was found at ~ 5 mol% of ThO_2 by Latta *et al.* [30] and Böhler *et al.* [32].

3.4 Melting temperatures of $(Th,Pu)O_2$ MOX

In an ideal case of no interaction between the solution end members, the ideal solution solidus and liquidus lines of the binary high-temperature phase diagram are solely defined by the enthalpies of fusion and the melting temperatures of the two end members, as shown in **Figure 6** for ThO_2-PuO_2 MOX. **Figure 6** shows two ideal solidus-liquidus curves, generated by taking into account two different melting points of PuO_2 as reported by Bakker *et al.* [46] and Bruycker *et al.* [20]. In this definition it is assumed that the heat capacity is same for solid and liquid phases in the vicinity of melting and only configurational entropy is contributing to the Gibbs free energy. **Figure 6** also compares our MD calculated melting temperatures with the solidification temperatures measured by Böhler *et al.* [33] using a laser heating approach combined with fast pyrometry in a thermal arrest method, to determine the melting/solidification phase transition in mixed (PuO_2 + ThO_2) at high temperature. Our melting temperatures are in good agreement for the ThO_2 rich part of the phase diagram compared to the ideal solidus line and experimentally determined values by Böhler *et al.* [33]. In the PuO_2 rich part, MD values underestimate (by 200-300 K) the ideal solidus line as our MD calculated melting temperature value of pure PuO_2 is underestimated by 200 K, compared to the experimentally determined value by Bruycker *et al.* [20]. On the other hand, the MD values overestimate (by 50-100 K) the ideal solidus behavior as reported by Bakker *et al.* [46]. The MD

calculations suggest that the melting temperature of PuO_2-5 atom% ThO_2 is lower than pure PuO_2 and PuO_2-15 atom% ThO_2. This result is in agreement with a previous set of experimental melting temperatures by Böhler *et al.* [33], which are consistent with a minima in the phase diagram at ~ 5 mol% of ThO_2.

3.5 Enthalpy and density variation of Th rich $(Th,U)O_2$ and $(Th,Pu)O_2$ MOX

The MD calculated changes in enthalpy (H(T)-H(300 K)) and density of $Th_{0.9375}U_{0.0625}O_2$, $Th_{0.875}U_{0.125}O_2$, $Th_{0.8125}U_{0.1875}O_2$, $Th_{0.75}U_{0.25}O_2$ and $Th_{0.6875}U_{0.3125}O_2$ for both solid and liquid phases were fitted to equations (7)-(8) as well as (9)-(10) and fitting coefficients are listed in **Tables 4** and **5**. **Figure 7** compares the MD calculated change in enthalpy (H(T)-H(300 K)) values of (a) $Th_{0.9375}U_{0.0625}O_2$, (b) $Th_{0.875}U_{0.125}O_2$, (c) $Th_{0.8125}U_{0.1875}O_2$ and (d) $Th_{0.6875}U_{0.3125}O_2$ MOX upon heating in the 300-6000 K range, (*i.e.* for both solid and liquid phases) and cooling in the 6000-2000 K range, with experimentally available data for $Th_{0.98}U_{0.06}O_2$, $Th_{0.92}U_{0.08}O_2$, $Th_{0.90}U_{0.10}O_2$, $Th_{0.85}U_{0.15}O_2$, $Th_{0.80}U_{0.20}O_2$ and $Th_{0.70}U_{0.30}O_2$ [23,24,45]. MD calculated values of enthalpy increments are in good agreement with experimental values at nearby compositions. **Figure 7** also shows the variation of fitting equations obtained from our MD calculated data set. No experimental data are available for liquid $(Th,U)O_2$ MOX.

Similarly, MD calculated changes in enthalpy (H(T)-H(300 K)) and density of $Th_{0.97}Pu_{0.03}O_2$, $Th_{0.95}Pu_{0.05}O_2$, $Th_{0.92}Pu_{0.08}O_2$, $Th_{0.80}Pu_{0.20}O_2$ and $Th_{0.70}Pu_{0.30}O_2$ for both solid and liquid phase were fitted to equations (7)-(8) as well as (9)-(10) and fitting coefficients are listed in **Tables 4** and **5**. **Figure 8** compares the MD calculated change in enthalpy (H(T)-H(300 K)) values of (a) $Th_{0.97}Pu_{0.03}O_2$ (b) $Th_{0.92}Pu_{0.08}O_2$ (c) $Th_{0.80}Pu_{0.20}O_2$ and (d) $Th_{0.70}Pu_{0.30}O_2$ $Th_{0.9375}U_{0.0625}O_2$, (b) $Th_{0.875}U_{0.125}O_2$, (c) $Th_{0.8125}U_{0.1875}O_2$ and (d) $Th_{0.6875}U_{0.3125}O_2$ MOX upon heating in the 300-6000 K range (*i.e.* for both solid and liquid phases) and cooling in the 6000-2000 K range, with experimentally available data [34]. MD calculated values of enthalpy increments are in good agreement with experimental values.

4. Discussion

4.1 Melting Temperatures ThO_2, UO_2 and PuO_2

Table 2 reports the experimental melting point values for ThO_2, which vary from 3573 K to 3660 K [6-10]. Initially, Lambertson *et al.* [8] predicted the melting point of 3623 K by extrapolating the melting point data of $(Th,U)O_2$ compositions corresponding to zero UO_2 content. Further

refinement was carried out by introducing corrections for the liquidus/solidus curve to incorporate a curvature correction for the pure ThO_2 end, to that of the pure UO_2 end of the temperature-composition diagram. Their final recommended value was 3573 K. However, Rand *et al.* [7] argued that the curvature corrections made by other researchers on the ThO_2 or UO_2 rich sides of the temperature composition curve need not be the same, because the loss of 'O' from UO_2 in the UO_2-rich side might be different from that of the ThO_2 rich side and hence recommended a value of 3643 ± 30 K. Ronchi *et al.* [9] recently measured the melting temperature of ThO_2 experimentally (under both stoichiometric and hypostoichiometric conditions) by heating a spherical sample with four symmetrically spaced pulsed Nd YAG lasers and observing the cooling/heating curve with time. For stoichiometric ThO_2, the measured melting point was 3651 ± 17 K [9] and their data is consistent with the data generated by Benz *et al.* [6] (3660 ± 100 K), which is also close to the value of Rand *et al.* [7]. All these values are markedly different from those of Lambertson *et al.* [8]. It is also important to note that the curvature differences at the uranium- and thorium-rich side of the temperature versus composition diagram can be attributed to the loss of oxygen. Furthermore, measurements of the cooling curves of molten ThO_2 and $ThO_{1.98}$ by Ronchi *et al.* [9] reveal that the stoichiometric compound melts congruently at 3651 K, while the hypostoichiometric oxide displays a liquidus at 3628 K and a solidus transition at 3450 K. Recently, Böhler *et al.* [10] revisited the high temperature phase diagram of ThO_2-UO_2 using a laser heating approach combined with fast pyrometry via a thermal arrest method and recommended a melting temperature of 3624 ± 108 K for ThO_2. Finally, our MD calculated value, which lies between 3650 K and 3675 K, is consistent with the data of Rand *et al.* [7], Ronchi *et al.* [9], Benz *et al.* [6], Böhler *et al.* [10] and even the upper value due to Lombertson *et al.* [8].

Experimentally reported melting temperatures of UO_2 vary from 3050 K to 3138 K (**Table 2**) [11-18]. The melting point of UO_2 given in MATPRO [15] is 3113.15 K, based on the equations for the solids and liquids boundaries of the UO_2-PuO_2 phase diagram given by Lyon *et al.* [11]. The recommended value by ORNL [17] for $UO_{2.00}$ is 3120 ± 30 K. In recent experimental measurements of the heat capacity of liquid UO_2, using laser heating of a UO_2 sphere, Ronchi *et al.* [13] made several measurements of the freezing temperature of UO_2 on different samples. For specimens in an inert gas atmosphere with up to 0.1 bar of oxygen, they obtained melting points in the interval 3070 ± 20 K. Higher melting temperatures (3140 ± 20 K) were obtained for samples in an inert gas atmosphere without oxygen. The variation in melting temperature is in accordance with the expected lower oxygen-to-uranium (O/U) ratio in the latter samples. The melting point of UO_2 drops on variation of the O/M

ratio away from stoichiometry: for example, if the melting point of stoichiometric UO_2 is 3138 K, its value drops to 2698 K at an O/U ratio of 1.68 and to 2773 K at an O/U ratio of 2.25 [13]. Thus, our MD calculated melting temperature, which lies between 3050 K and 3075 K, is in fairly consistent with experimental data available in the literature for stoichiometric UO_2.

The determine melting point of PuO_2 a series of measurements were performed by Lyon *et al.* [11] using the thermal arrest technique and induction heating of tungsten-encapsulated samples. Also, some other researchers [11, 14-17] studied melting of PuO_2 and reported values in the range 2663-2718 K (**Table 2**), using combined visual detection of melting with a variety of experimental setups, including flame melting under a controlled atmosphere. The recommended value by ORNL [17] for for $PuO_{2.00}$ is 2701 ± 35 K. Kato *et al.* [19] reported the melting temperature of $PuO_{2.00}$ as 2843 K. Recently, Bruycker *et al.* [20] studied the melting temperature of stoichiometric PuO_2 by fast laser heating and multi-wavelength pyrometry. The transition temperatures obtained by this technique (3017 ± 28 K) are in disagreement with those previously proposed on the basis of more traditional measurements. The principal issue in those old measurements was the extensive interaction between sample and crucible during heat treatments which resulted in lower phase transition temperatures. The recent laser heating method [19,20] has the advantages of much shorter heating duration and quasi-containerless conditions and avoids most of the typical problems of traditional furnace techniques. Our MD calculated melting temperature, which lies between 2800 K and 2825 K, is lower than the melting point reported by Bruycker *et al.* [20] and higher than the recommended value by ORNL [17] but matches well with the value reported by Kato *et al.* [19].

4.2 Enthalpy and density variation of ThO_2, UO_2 and PuO_2

The MD calculated change in enthalpy (H(T)-H(300 K)) values of defect-free UO_2 upon heating match very well upto 2000 K. The underestimation of values from 2000 K to melting can be attributed to the Schottky defects and contribution from the electronic defects, which is not taken into account explicitly in these MD simulations using one-phase approach. Previously, Harding *et al.* [48] reporting on the anomalous specific heat of UO_2 at high temperatures suggested that there is a source of entropy, of the order of 10 cal/mol. K. The calculations in their paper show that it is highly unlikely that Frenkel defects on the anion sub-lattice can provide more than a small proportion of this. However, the contribution from electronic defects is large and could account for most of this volume. In their paper Harding *et al.* [48], considered only one small polaron reaction: $2U^{4+} \rightarrow U^{3+} + U^{5+}$. It is apparent that

there are others, which, although having a higher activation energy may make significant contributions close to the melting point.

Ronchi *et al.* [49] calculated the contributions from each physical process to the heat capacity to compare with available experimental data and provided an excellent description of the theoretical understanding. They found that from room temperature to 1000 K, the increase in heat capacity is governed by the harmonic lattice vibrations, which may be approximated by a Debye model. Between 1000 and 1500 K, the heat capacity increase arises from the anharmonicity of the lattice vibrations as evidenced in thermal expansion. The increased heat capacity from 1500 to 2670 K is due to the formation of lattice and electronic defects with the main contribution from Frenkel defects. Above the λ-phase transition, the Frenkel defect concentration becomes saturated and Schottky defects become important. Moreover, spin-phonon scattering plays a pivotal role in the low temperature thermal properties of UO_2 but not in ThO_2 [50].

From our MD calculated H(T)-H(300) versus temperature data, the enthalpy of fusion is calculated from the width of the discontinuity in the enthalpy axis and it is compared with other experimental values in **Table 3**. Fink *et al.* [25] estimated the specific heat C_p(liquid) to be 61.76 J K^{-1} mol^{-1} for liquid ThO_2, which is adopted here. Then if the entropy of fusion is assumed to be identical to that of UO_2 (24 J K^{-1} mol^{-1}), it yields an enthalpy of fusion for ThO_2 = 88±6 kJ mol^{-1}. The enthalpy of fusion for PuO_2 is estimated, assuming that the entropy of fusion is identical to that of UO_2 (22.4 J K^{-1} mol^{-1}), yielding an enthalpy of fusion = 64± 6 kJ mol^{-1}. MD calculated enthalpy of fusion values are consistently lower than experimental values. It has been established in this kind of solid dioxides that the formation of oxygen defects, and in particular of Frenkel pairs, leads to an abrupt increase of the heat capacity as temperature approaches the melting point [51,52]. In the case of UO_2 and ThO_2, even a pre-melting order-disorder ‘‘lambda’’ transition has been proposed by certain authors [53-55]. One-phase approach to calculate enthalpy increments and density does not take into account these effects, resulting in overall underestimation of MD calculated enthalpy of fusion values compared to experimental values.

Ideally, discontinuous jump in the enthalpy *vs* temperature plot signifies melting and/or solidification of the solid-liquid transformation. The temperature at which the discontinuous jump appears should be melting and/or solidification temperature. **Figure 2, 3** and **4** shows high melting/solidification temperature by several hundred kelvin compared to equilibrium melting points predicted by two-phase simulations. At this point it is important to note that, the one phase approach is

employed in the calculation of enthalpy increments and density as one phase approach is computationally less expansive and easy to implement in the simulations compared to two phase approach. In one phase method, the supercell is subjected to incremental heating under the NPT ensemble until melted. Similarly, the liquid phase is subjected to the same incremental cooling until recrystallization. The solid-liquid phase transformation is a first order reaction and associated with hysteresis. Based on classical nucleation theory, there is a sudden jump in volume (or density) upon melting at T_+ (superheating temperature) in a heating simulation of a solid, and there is a drop in volume (or density) at T_- (supercooling temperature) due to fusion in a cooling simulation of a liquid. The density-temperature curve (**Figure 2, 3, 4**) reveals the hysteresis effects for the MD simulations of a solid and a liquid. Compared to the hysteresis approach, the two-phase approach is more meaningful and models a first order transformation where two phases co-exist with an interface between them. The hysteresis approach lacks this feature. The melting temperature T_m is obtained from the solid-liquid coexistence, where the free energies of solid and liquid states becomes equal. So we adopted the two-phase simulation method to calculate the high temperature phase diagram of $(Th,U)O_2$ and $(Th,Pu)O_2$ MOX. Superheating and supercooling phenomena are common in MD simulations of solid-liquid phase transformation [56-58].

4.3 Melting temperatures of $(Th,U)O_2$ and $(Th,Pu)O_2$ MOX

High temperature phase diagram studies of the ThO_2-UO_2 MOX system have previously been reported by Lambertson *et al.* [21] using a quench technique, whereas Latta *et al.* [30] applied a thermal arrest method to determine the liquidus and solidus of MOX. The measurements of Latta *et al.* [30] in the 0-17 mole % ThO_2 also show deviation from the ideal liquidus-solidus curve and this behavior would be consistent with a shallow minimum around 5 mol.% ThO_2. Moreover, the high temperature phase diagram of ThO_2-UO_2 MOX can be constructed with the help of the melting points and enthalpies of fusion of the end members, assuming these complete solution binaries are ideal solid solutions, (*i.e.* no change in volume or enthalpy on mixing [31]). Assuming an ideal mixing for both the solid and the liquid (ThO_2+UO_2) solutions, the solidus and liquidus line can be obtained by solving the following system of equations:

$$\Delta H_m(ThO_2)\left(\frac{1}{T_m(ThO_2)}-\frac{1}{T}\right)=R\ln\left(\frac{1-x_l}{1-x_s}\right) \qquad (15)$$

$$\Delta H_m(UO_2)\left(\frac{1}{T_m(UO_2)}-\frac{1}{T}\right)=R\ln\left(\frac{x_l}{x_s}\right)$$

R is the ideal gas constant (8.314462 kJ. K^{-1}. Mol^{-1}), x_s and x_l are the UO_2 mole fractions on the, respective, solidus and liquidus curves at a given absolute temperature T ($T_m(UO_2) < T < T_m(ThO_2)$). T_m and ΔH_m are the melting temperatures and enthalpies of fusion of the two end members, respectively. As there is no direct experimental measurement of the heats of fusion for ThO_2 or ThO_2–UO_2 solid solutions, the most probable value is that of Fink *et al.* [27] for UO_2 (i.e. 74.8 ± 1 kJ/mol) and the recommended value for ThO_2 is 90.8 kJ/mol [1]. Recently, Böhler *et al.* [31] revisited the high-temperature phase diagram of ThO_2-UO_2 using a laser heating approach combined with fast pyrometry in a thermal arrest method. According to their study, low additions of ThO_2 to UO_2 result in a slight decrease of the solidification temperature and this behviour would be consistent with a minimum at 3098 K around a composition of 5 mol% ThO_2. The solid/liquid transition temperature was thereafter observed to increase with increasing ThO_2 fraction.

The solidus-liquidus curve in the uranium rich side is expected to influence by the following facts:

a) The derivation of ideal solidus-liquidus line (from equation (15)) assumes that the heat capacity of the end members is independent of temperature and composition in the vicinity of the melting transition. On the contrary, previous experimental studies reported abrupt increase of specific heat due to formation of Frenkel pairs and order-disorder pre-melting transitions [51-55].

b) The creation of oxygen defects is actually likely to occur in uranium-rich samples, because U has a partially filled 5-f electron shell and can therefore easily assume the valences +3, +4, +5 and +6 even in the condensed oxide phases [59].

c) Since at high temperatures uranium dioxide can accommodate in the fcc lattice both oxygen interstitials and vacancies over a wide stoichiometry range (at least, $1.5 \leq O/U \leq 2.25$), important variations of the melting point with stoichiometry are expected in conjunction with the appearance of an oxygen solubility gap when solid solutions $UO_{2\pm x}$ are melted [60].

The minimum in the uranium rich side of ThO_2-UO_2 phase diagram is an outcome of above mentioned effects. Incorporation of all these effects in the current state-of-the MD simulation methodologies is difficult. Two-phase simulations employed in this study to calculate melting temperature of ThO_2, UO_2 and MOX indirectly incorporate the effect of lattice defects (mostly Frenkel

defects). Non-stoitiometry effect requires U^{+3}- O^{-2} and U^{+3} - O^{-2} interactions to be incorporated in the potential data set efficiently.

5. Conclusion

The melting behavior of pure ThO_2, UO_2 and PuO_2 as well as $(Th,U)O_2$ and $(Th,Pu)O_2$ MOX has been studied using MD simulations at ambient pressure using newly developed interatomic potentials that combine Coulomb, Buckingham, Morse and many-body functional forms. It was found that:

1) The MD calculated MT of ThO_2 and UO_2 lie between 3650-3675 K and 3050-3075 K, respectively, which match well with experiment. For PuO_2, the MD calculated MT value, which lies between 2800-2825 K, falls between previously determined older experimental values and a recently determined value by Bruycker *et al.* [20]. Moreover, MD calculated values of enthalpy increment for the solid phase of UO_2 match well with experimental values but overestimate (by ~ 50 kJ mol^{-1}) the value for the liquid phase. Nevertheless the calculated density variation as a function of temperature for both the solid and liquid phases is in good agreement with experiment. Our study reports enthalpy increment values of ThO_2 and PuO_2 for solid as well as liquid phases, which were not reported earlier.
2) Enthalpy of fusion values for ThO_2, UO_2 and PuO_2 are calculated from the width of the enthalpy discontinuity and calculated values are lower than experimental values as the lattice and electronic defect contribution to the enthalpy is not taken into account in our one-phase simulations.
3) The MD calculated MT of $(Th,U)O_2$ and $(Th,Pu)O_2$ MOX show good agreement with the ideal solidus line in the Th rich part of the phase diagram. The ideal solidus line is, however, underestimated by ~ 50 K for $(Th,U)O_2$ in the UO_2 rich parts of the phase diagram. Importantly, our study would be consistent with a minima around 5 atom% of ThO_2 in the high temperature phase diagram of $(Th,Pu)O_2$ MOX.
4) MD calculated enthalpy increments as a function of temperature for ThO_2 rich $(Th,U)O_2$ and $(Th,Pu)O_2$ MOX are in good agreement with experiment.

Acknowledgment

We thank the EPSRC for funding as part of the INDO-UK project (grant code EP/K00817X/1). Computational facilities and support were provided by High Performance Computing Centres at Bhabha Atomic Research Centre and Imperial College London.

References

[1] International Atomic Energy Agency. Thorium fuel cycle-potential benefits and challenges, IAEA-TECDOC-1450, IAEA, Vienna, 2005.

[2] R.K. Sinha, A. Kakodkar, Nucl. Eng. Des. 236 (2006) 683-700.

[3] Thermophysical properties database of materials for light water reactors and heavy water reactors IAEA-TECDOC-1496. Australia: International Atomic Energy Agency, June 2006.

[4] P.S. Ghosh, P.S. Somayajulu, A. Arya, G.K. Dey, B.K. Dutta, Journal of Alloys and Compounds, 638 (2015) 172-181

[5] P.S. Ghosh, P.S. Somayajulu, K. Krishnan, N. Pathak, A. Arya, G.K. Dey, Journal of Alloys and Compounds, 650 (2015) 165-177

[6] R. Benz, J. Nucl. Mater. 29 (1969) 43–49.

[7] M.H. Rand (1975) Thorium: physico-chemical properties of its compounds and alloys. Atom Energy Rev 5:35

[8] W.A. Lambertson, M.H. Mueller, F.H. Gunzel, J. Am. Ceram. Soc 36 (1953) 397–399.

[9] C. Ronchi, J.P. Hiernaut, J. Alloys Compd. 240 (1996) 179–185.

[10] R. Böhler, A. Quaini, L. Capriotti, P. Çakır, O. Beneš, K. Boboridis, A. Guiot, L. Luzzi, R. Konings, D. Manara, J. Alloys & Compd. 616 (2014) 5–13.

[11] W.L. Lyon, W.E. Baily, J. Nucl. Mater. 22 (1967) 332–339.

[12] R.E. Latta, R.E. Fryxell, J. Nucl. Mater. 35 (1970) 195–210.

[13] C. Ronchi, J.P. Hiernaut, R. Selfslag, G.J. Hyland, Nucl Sci Eng 113 (1993) 1–19.

[14] M.G. Adamson, E.A. Aitken, R.W. Caputi, J. Nucl. Mater. 130 (1985) 349–365.

[15] D.T. Hagrman, MATPRO - A library of materials properties for Light Water Reactor accident Analysis. SCDAP/RELAP5/MOD 3.1/Code manual, Vol. 4. MATPRO, USNRC Report NUREG/CR-6150 (EGGG-2720) (1995).

[16] J. Komatsu, T. Tachibana, K. Konashi, J. Nucl. Mater. 154 (1988) 38–44.

[17] S.G. Popov, J.J. Carbajo, V.K. Ivanov, G.L. Yoder, Thermophysical properties of MOX and UO_2 fuels including its effects of irradiation. ORNL/TM-2000/351, Oak Ridge National Laboratory, Oak Ridge (2000).

[18] R. Böhler, M. Welland, D. Prieur, P. Çakır, T. Vitova, T. Pruessmann, I. Pidchenko, C. Hennig, C. Guéneau, R. , D. Manara, J. Nucl. Mater. 448 (1–3) (2014) 330–339.

[19] M. Kato, K. Morimoto, H. Sugata, K. Konashi, M. Kashimura, T. Abe, Journal of Nuclear Materials 373 (2008) 237–245.

[20] F. De Bruycker, K. Boboridis, P. Pöml, R. Eloirdi, R.J.M. Konings, D. Manara, Journal of Nuclear Materials 416 (2011) 166–172.

[21] M. Hoch and H. L. Johnston, J. Phys. Chem. 65, 1184 (1961).

[22] D. F. Fischer, J. K. Fink, and L. Leibowitz, J. Nucl. Mater. 102, 220 (1981).

[23] R. Agarwal, R. Prasad, and V. Venugopal, J. Nucl. Mater. 322, 98 (2003).

[24] S. Dash, S. C. Parida, Z. Singh, B. K. Sen, and V. Venugopal, J. Nucl. Mater. 393, 267 (2009).

[25] J. K. Fink, M. G. Chasanov, and L. Leibowitz, Technical Report ANLCEN-RSD–77-1 (Argonne National Laboratory, 1977).

[26] A.C. Momin and Karkhanvala, High Temp. Sci., 10 (1978) 45.

[27] J.K. Fink, M.G. Chasanov, and L. Leibowitz, *Thermophysical Properties of Uranium Dioxide,* J. Nucl. Mater.102 17-25 (1981).

[28] J.K. Fink, Journal of Nuclear Materials 279 (2000) 1±18.

[29] A. E. Ogard, Plutonium 1970 and Other Actinides (Metallurgical Society of the American Institute of Mining, New York, 1970), p. 78.

[30] R. E. Latta, E. C. Duderstadt and R. E. Fryxell, J. Nuc. Mat. 35 (1970) 347-349.

[31] J. Belle, R.M. Berman (1984) Thorium dioxide: properties and nuclear applications. Naval Reactors Office, United State Department of Energy, Government Printing Office, Washington.

[32] R. Bohler, A. Quaini, L. Capriotti, P. Cakır, O. Beneš, K. Boboridis, A. Guiot, L. Luzzi, R.J.M. Konings, D. Manara, Journal of Alloys and Compounds 616 (2014) 5–13.

[33] R. Bohler, P. Cakır, O. Beneš, H. Hein, R.J.M. Konings, D. Manara, J. Chem. Thermodynamics 81 (2015) 245–252.

[34] O.S. Vaˇlu, O. Beneš, R.J.M. Konings, H. Hein, J. Chem. Thermodynamics 68 (2014) 122–127.

[35] MWD Cooper, MJD Rushton, RW Grimes, Journal of Physics: Condensed Matter 26 (2014) 105401 (10 pp).

[36] M.W.D. Cooper, S.T. Murphy, M.J.D. Rushton, R.W. Grimes, Journal of Nuclear Materials 461, 206-214

[37] MWD Cooper, ST Murphy, PCM Fossati, MJD Rushton, RW Grimes, Proceedings of the Royal

Society of London A: Mathematical, Physical and Engineering Sciences 470 (2014) 20140427

[38] A. Zunger, S. Wei, L.G. Ferreira, and J.E. Bernard, Phys. Rev. Lett. 65 (1990) 353-356.

[39] J. von Pezold, A. Dick, M. Friak, J. Neugebauer, Phys. Rev. B 81 (2010) 094203.

[40] P.S. Somayajulu, P.S. Ghosh, A. Arya, K.V. Vrinda Devi, D.B. Sathe, J. Banerjee, K.B. Khan, G.K. Dey, B.K. Dutta, *Journal of Alloys and Compounds 664 (2016) 291-303.*

[41] P.S. Somayajulu, P.S. Ghosh, J. Banerjee, K.L.N.C. Babu, K.M. Danny, B.P. Mandal, T. Mahata, P. Sengupta, S.K. Sali, A. Arya, *Journal of Nuclear Materials 467 (2015) 644-659.*

[42] S. Plimpton, J. Comput. Phys. 117 (1995) 1.

[43] P.P. Ewald, Ann. Phys. 64 (1921) 253.

[44] Laalitha SI Liyanage, Seong-Gon Kim, Jeff Houze, Sungho Kim, Mark A. Tschopp, M. I. Baskes, M. F. Horstemeyer, Phys. Rev. B 89 (2014) 094102.

[45] D.F. Fischer, J.K. Fink, L. Leibowitz, Journal of Nuclear Materials 118 (1983) 342-348.

[46] K. Bakker, E.H.P. Cordfunke, R.J.M. Konings, R.P.C. Schram, J. Nucl. Mater. 250 (1997) 1–12.

[47] M.J. Qin, M W D Cooper, E Y Kuo, M J D Rushton, R W Grimes, G R Lumpkin and S C Middleburgh, Journal of Physics: Condensed Matter 26 (2014) 495401 (9 pp)

[48] J.H. Harding, P. Masri and A.M. Stoneham, Journal of Nuclear Materials 92 (1980) 73-78

[49] C. Ronchi, G.J. Hyland, J. Alloys Compounds, 213/214 (1994) 159.

[50] K. Gofryk, S. Du, C. Stanek, J. Lashley, X.-Y. Liu, R. Schulze, J. Smith, D. Safarik, D. Byler, K. McClellan, B. Uberuaga, B. Scott, D. Andersson, Nat. Commun. 5 (2014) 4551.

[51] R.J.M. Konings, O. Benes, J. Phys. Chem. Solids 74 (2013) 653–655.

[52] M. Chollet, J. Léchelle, R.C. Belin, J.-C. Richaud, J. Appl. Cryst. 47 (2014) 1008-1015.

[53] C. Ronchi, M. Sheindlin, M. Musella, G. Hyland, J. Appl. Phys. 85 (1999) 776-789.

[54] C. Ronchi, J.-P. Hiernaut, J. Alloys Compd. 240 (1996) 179–185.

[55] A.V. Lunev, B.A. Tarasov, J. Nucl. Mater. 415 (2011) 217–221.

[56] Sheng-Nian Luo, Alejandro Strachan, and Damian C. Swift, The Journal of Chemical Physics 120 (2004) 11640.

[57] Wenjin Zhang, Yufeng Peng and Zhongli Liu, AIP Advances 4 (2014) 057110.

[58] H. Xiao, C. Long, X. Tian, H. Chen, Materials & Design 96 (2016) 335-340.

[59] H. Idriss, Surf. Sci. Rep. 65 (2010) 67-109.

[60] D. Manara, C. Ronchi, M. Sheindlin, M. Lewis, M. Brykin, Journal of Nuclear Materials 342 (2005) 148–163.

Tables

Table 1: Pair and multisite correlation functions of SQS-96 structures for mimicking ideal random $Th_{1-x}U_xO_2$ solid-solution (x = 1/6, 2/16, 3/16, 4/16, 5,16 and 6/16).

$\Pi_{k,m}$	Composition $Th_{1-X}U_xO_2$					
	x = 1/16 (0.0625)	x = 2/16 (0.125)	x = 3/16 (0.1875)	x = 4/16 (0.25)	x = 5/16 (0.3125)	x = 6/16 (0.375)
$\Pi_{2,1}$	0.77083	0.56250	0.39583	0.25000	0.14583	0.08333
$\Pi_{2,2}$	0.75000	0.58333	0.41667	0.25000	0.08333	0.00000
$\Pi_{2,3}$	0.75000	0.54167	0.35417	0.22917	0.12500	0.04167
$\Pi_{2,4}$	0.75000	0.50000	0.33333	0.16667	0.08333	0.00000
$\Pi_{2,5}$	0.77083	0.56250	0.39583	0.25000	0.14583	0.08333
$\Pi_{2,6}$	0.75000	0.50000	0.25000	0.00000	0.25000	0.50000
random	0.76562	0.56250	0.39062	0.25	0.14062	0.0625
$\Pi_{3,1}$	0.68750	0.4375	0.2500	0.1250	0.0625	0.03125
$\Pi_{3,2}$	0.66667	0.43750	0.27083	0.10417	0.02083	0.02083
$\Pi_{3,3}$	0.66667	0.40625	0.23958	0.12500	0.06250	0.02083
$\Pi_{3,3}$	0.64583	0.38542	0.18750	0.09375	0.03125	0.01042
$\Pi_{3,3}$	0.64583	0.41667	0.25000	0.12500	0.04167	0.00000
$\Pi_{3,3}$	0.62500	0.41667	0.22917	0.12500	0.04167	0.02083
$\Pi_{3,3}$	0.62500	0.37500	0.15625	0.09375	0.03125	0.00000
random	0.66992	0.42188	0.24414	0.125	0.05273	0.015625
$\Pi_{4,1}$	0.62500	0.37500	0.12500	0.00000	0.12500	0.12500
$\Pi_{4,2}$	0.60417	0.35417	0.18750	0.04167	0.02083	0.02083
$\Pi_{4,3}$	0.58333	0.33333	0.16667	0.08333	0.00000	0.08333
random	0.58618	0.31641	0.15259	0.0625	0.01978	0.00391

Table 2: MD calculated melting temperatures of pure ThO_2, UO_2 and PuO_2 are compared with experimentally measured values available in the literature.

System	MD calculated temperature range (K)	Experimental values (K)
ThO_2	3650-3675	3663 ± 100 Benz *et al.* [6] 3643 ± 30 Rand *et al.* [7] 3573 ± 100 Lambertson *et al.* [8] 3651 ± 17 Ronchi *et al.* [9] 3624 ± 108 Bohler *et al.* [10]
UO_2	3050-3075	3113 ± 20 Lyon *et al.* [11] 3138 ± 15 Latta *et al.* [12] 3075 ± 30 Ronchi *et al.* [13] 3120 ± 30 Adamson *et al.* [14] 3,113.15 MATPRO [15] 3138 ± 15 Komatsu *et al.* [16] 3120 ± 30 ORNL [17] 3050 ± 55 Böhler *et al.* [18]
PuO_2	2800-2825	2663 ± 20 Lyon *et al.* [11] 2701 ± 35 Adamson *et al.* [14] 2647 MATPRO [15] 2718 Komatsu *et al.* [16] 2701 ± 35 ORNL [17] 2843 Kato *et al.* [19] 3017 ± 28 Bruycker *et al.* [20]

Table 3: MD calculated enthalpy of fusion of pure ThO_2, UO_2 and PuO_2 are compared with experimentally measured values available in the literature.

System	MD calculated enthalpy of fusion (this study) kJ/mol	Experiments (kJ/mol)
ThO_2	63.85	88 ± 6, Fink et al. [25] 90.8 **,** IAEA-TECDOC 1496 (2006) [1]
UO_2	58.94	74.8, Fink et al. [27] 70.0 ± 4, Fink et al. [28] 70.0, MATPRO [15]
PuO_2	43.21	64± 6 [29]

Table 4: MD calculated enthalpy increments (in J/mole) of solid and liquid phases of $(Th,U)O_2$ and $(Th,Pu)O_2$ MOX are fitted to equation (7) and (8), respectively and coefficients are enlisted.

MOX	Solid phase enthalpy (300 K – melting point) $H(T)-H(300)=C_1\theta\left[\left(e^{\theta/T}-1\right)^{-1}-\left(e^{\theta/300}-1\right)^{-1}\right]+C_2\left[T^2-(300)^2\right]+C_3e^{-\beta/T}$	Liquid phase enthalpy (melting point - 6500 K) $H(l,T)-H(s,300)=C_1+C_2T-C_3/T$
ThO_2	C_1 = 99.391, θ = 637.205, C_2 = -8.129 × 10^{-3}, C_3 = 3.35847 × 10^6, β = 12228.3	C_1 = 4.24348 × 10^4, C_2 =100.961, C_3 = 9.8998 × 10^7
$Th_{0.9375}U_{0.0625}O_2$	C_1 = 110.222, θ = 731.487, C_2 = -12.804 × 10^{-3}, C_3 = 3.27702 × 10^6, β = 11344.4	C_1 = 3.4106 × 10^4, C_2 =102.162, C_3 = 9.8998 × 10^7
$Th_{0.875}U_{0.125}O_2$	C_1 = 115.830, θ = 795.683, C_2 = -15.229 × 10^{-3}, C_3 = 3.07690 × 10^6, β = 10780.7	C_1 = 3.53084 × 10^4, C_2 =101.469, C_3 = 9.8996 × 10^7
$Th_{0.8125}U_{0.1875}O_2$	C_1 = 117.105, θ = 803.765, C_2 = -15.779 × 10^{-3}, C_3 = 3.13532 × 10^6, β = 10737.2	C_1 = 2.98641 × 10^4, C_2 =102.254, C_3 = 9.8997 × 10^7
$Th_{0.75}U_{0.25}O_2$	C_1 = 117.565, θ = 810.081, C_2 = -16.092 × 10^{-3}, C_3 = 2.97057 × 10^6, β = 10487.7	C_1 = 3.17325 × 10^4, C_2 =101.673, C_3 = 9.9000 × 10^7
$Th_{0.6875}U_{0.3125}O_2$	C_1 = 132.225, θ = 865.31, C_2 = -23.5569 × 10^{-3}, C_3 = 3.03601 × 10^6, β = 9637.35	C_1 = 4.2448 × 10^4, C_2 = 99.1047, C_3 = 9.9007 × 10^7
$Th_{0.97}Pu_{0.03}O_2$	C_1 = 103.303, θ = 715.159, C_2 = -9.50969 × 10^{-3}, C_3 = 3.97188 × 10^6, β = 12543.8	C_1 = 3.32842 × 10^4, C_2 = 101.59, C_3 = 9.89886 × 10^7

$Th_{0.95}Pu_{0.05}O_2$	C_1 = 114.168, θ = 798.406, C_2 = -14.1746 × 10^{-3}, C_3 = 3.79121 × 10^6, β = 11672.6	C_1 = 3.17318 × 10^4, C_2 = 101.363, C_3 = 9.90000 × 10^7
$Th_{0.92}Pu_{0.08}O_2$	C_1 = 117.924, θ = 805.625, C_2 = -16.1121 × 10^{-3}, C_3 = 3.52877 × 10^6, β = 11122.1	C_1 = 3.17322 × 10^4, C_2 = 101.415, C_3 = 9.90000 × 10^7
$Th_{0.80}Pu_{0.20}O_2$	C_1 = 118.129, θ = 798.347, C_2 = -16.9268 × 10^{-3}, C_3 = 3.03574 × 10^6, β = 10356.2	C_1 = 2.97335 × 10^4, C_2 = 100.395, C_3 = 9.89900 × 10^7
$Th_{0.70}Pu_{0.30}O_2$	C_1 = 101.116, θ = 647.798, C_2 = -9.52912 × 10^{-3}, C_3 = 2.95858 × 10^6, β = 11116.8	C_1 = 2.99031 × 10^4, C_2 = 99.4849, C_3 = 9.89999 × 10^7
PuO_2	C_1 = 238.77, θ = 1269.05, C_2 = -68.9664 × 10^{-3}, C_3 = 5.42283 × 10^6, β = 8740.69	C_1 = 3.08813 × 10^4, C_2 = 96.033, C_3 = 7.6837 × 10^7

Table 5: MD calculated density (in g/cm^3) of solid and liquid phases of $(Th,U)O_2$ and $(Th,Pu)O_2$ MOX are fitted to equation (9) and (10), respectively and coefficients are enlisted.

MOX	Solid phase density (300 K – melting point T_m) $\rho(T)=C_1+C_2T+C_3T^2+C_4T^3$	Liquid phase density (melting point T_m - 6500 K) $\rho(T)=C_1+C_2(T-T_m)$
ThO_2	C_1 = 10.0912, C_2 = -2.66141 x 10^{-4} C_3 = -0.456978 x 10^{-8}, C_4 = 1.12 x 10^{-11}	C_1 = 8.22764, C_2 = -7.35261 x 10^{-4}
$Th_{0.9375}U_{0.0625}O_2$	C_1 = 10.1478, C_2 = -2.582 x 10^{-4} C_3 = -0.52999 x 10^{-8}, C_4 = 0.94666 x 10^{-11}	C_1 = 8.37026, C_2 = -7.2469 x 10^{-4}
$Th_{0.875}U_{0.125}O_2$	C_1 = 10.2002, C_2 = -2.4073 x 10^{-4} C_3 = -2.1128 x 10^{-8}, C_4 = 0.66745 x 10^{-11}	C_1 = 8.23388, C_2 = -7.18225 x 10^{-4}
$Th_{0.8125}U_{0.1875}O_2$	C_1 = 10.2482, C_2 = -2.09567 x 10^{-4} C_3 = -4.77534 x 10^{-8}, C_4 = -1.6402 x 10^{-12}	C_1 = 8.27608, C_2 = -7.41197 x 10^{-4}
$Th_{0.75}U_{0.25}O_2$	C_1 = 10.3102, C_2 = -2.1423 x 10^{-4} C_3 = -4.9352 x 10^{-8}, C_4 = -1.4689 x 10^{-12}	C_1 = 8.29257, C_2 = -7.47047 x 10^{-4}
$Th_{0.6875}U_{0.3125}O_2$	C_1 = 10.357, C_2 = -1.85017 x 10^{-4} C_3 = -7.20112 x 10^{-8}, C_4 = -2.5823 x 10^{-12}	C_1 = 8.28532, C_2 = -7.27682 x 10^{-4}

$Th_{0.97}Pu_{0.03}O_2$	C_1 = 10.1003, C_2 = -2.2928 x 10^{-4} C_3 = -2.2473 x 10^{-8}, C_4 = 0.6232 x 10^{-11}	C_1 = 8.3892, C_2 = -7.3762 x 10^{-4}
$Th_{0.95}Pu_{0.05}O_2$	C_1 = 10.1777, C_2 = -2.5411 x 10^{-4} C_3 = -7.7185 x 10^{-8}, C_4 = 0.9219 x 10^{-11}	C_1 = 8.4166, C_2 = -7.2388 x 10^{-4}
$Th_{0.92}Pu_{0.08}O_2$	C_1 = 10.2065, C_2 = -2.4231 x 10^{-4} C_3 = -1.9516 x 10^{-8}, C_4 = 0.6956 x 10^{-11}	C_1 = 8.4241, C_2 = -7.2256 x 10^{-4}
$Th_{0.80}Pu_{0.20}O_2$	C_1 = 10.3781, C_2 = -2.0886 x 10^{-4} C_3 = -5.822 x 10^{-8}, C_4 = 0.0459 x 10^{-11}	C_1 = 8.66711, C_2 = -7.3751 x 10^{-4}
$Th_{0.70}Pu_{0.30}O_2$	C_1 = 10.5298, C_2 = -1.8369 x 10^{-4} C_3 = -8.9812 x 10^{-8}, C_4 = 0.7064 x 10^{-11}	C_1 = 8.5617, C_2 = -7.3224 x 10^{-4}
PuO_2	C_1 = 11.7581, C_2 = -3.229 x 10^{-4} C_3 = -1.0469 x 10^{-8}, C_4 = -1.6744 x 10^{-11}	C_1 = 9.9014, C_2 = -7.7439 x 10^{-4}

Figures

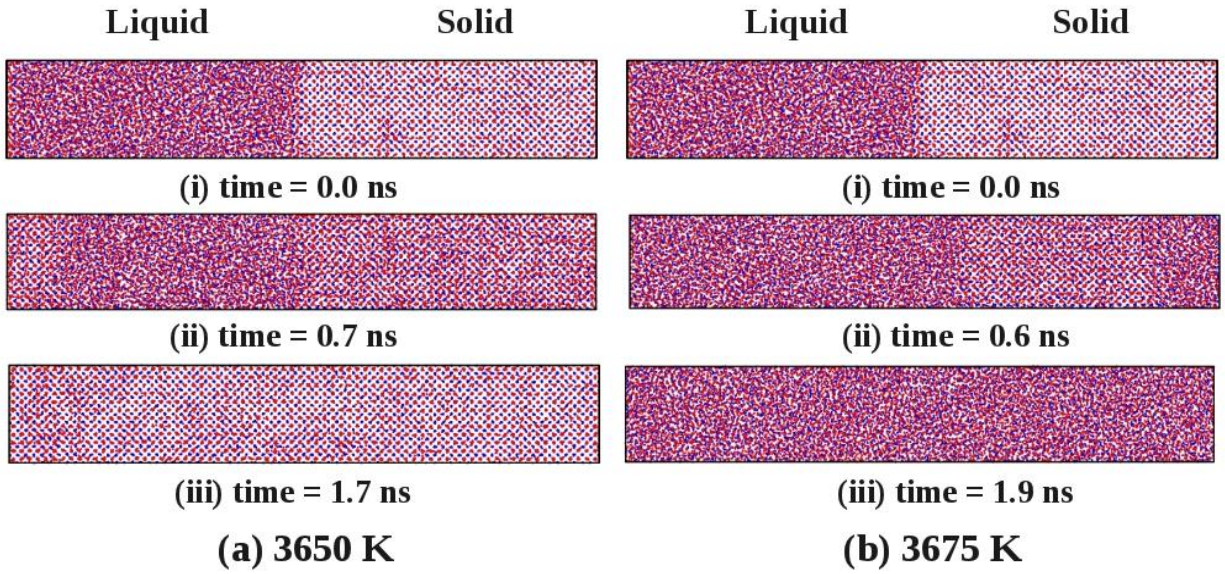

Figure 1: Snapshots of the two-phase MD simulation in the NPT ensemble with (a) T=3650 K (left panel) and (b) 3675 K (right panel). The red spheres represent O atoms and the blue spheres represent Th atoms. (a) Initial state of the simulation box, which contains both liquid and solid phases. (b) Intermediate state of the simulation box (at 0.6-0.7 ns), where the solid phase propagates to the liquid (at 3650 K) and liquid phase propagates to the solid phase (at 3675 K). (c) Final state of the simulation box (at 1.7-1.9 ns), when the entire system has turned into a solid phase (at 3650 K) and vice-verse (at 3675 K).

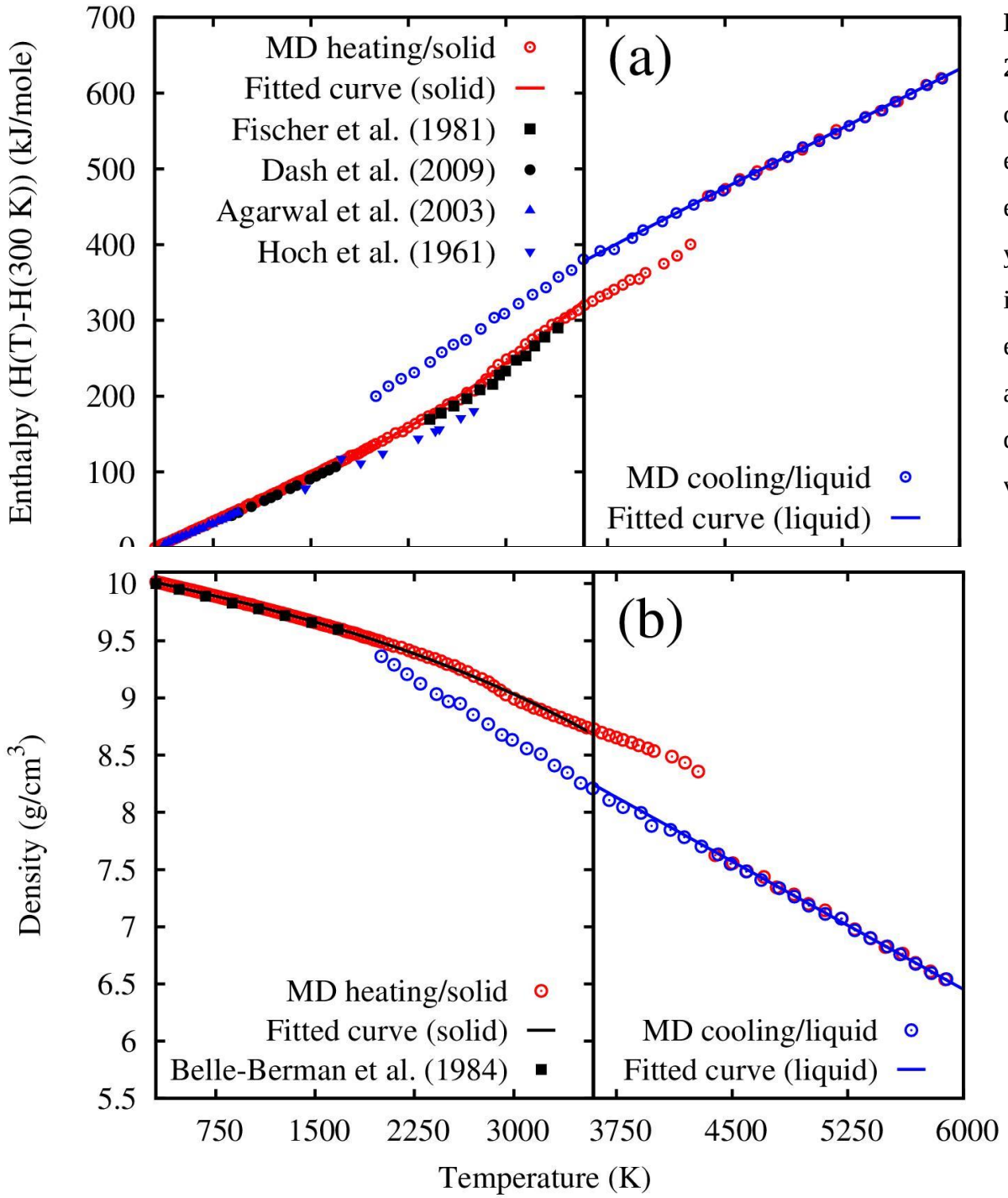

Figure 2: MD calculated enthalpy increments (a) and density variation (b) as a function of temperature in the 300-6000 K range

for ThO_2 are compared with experimental values.

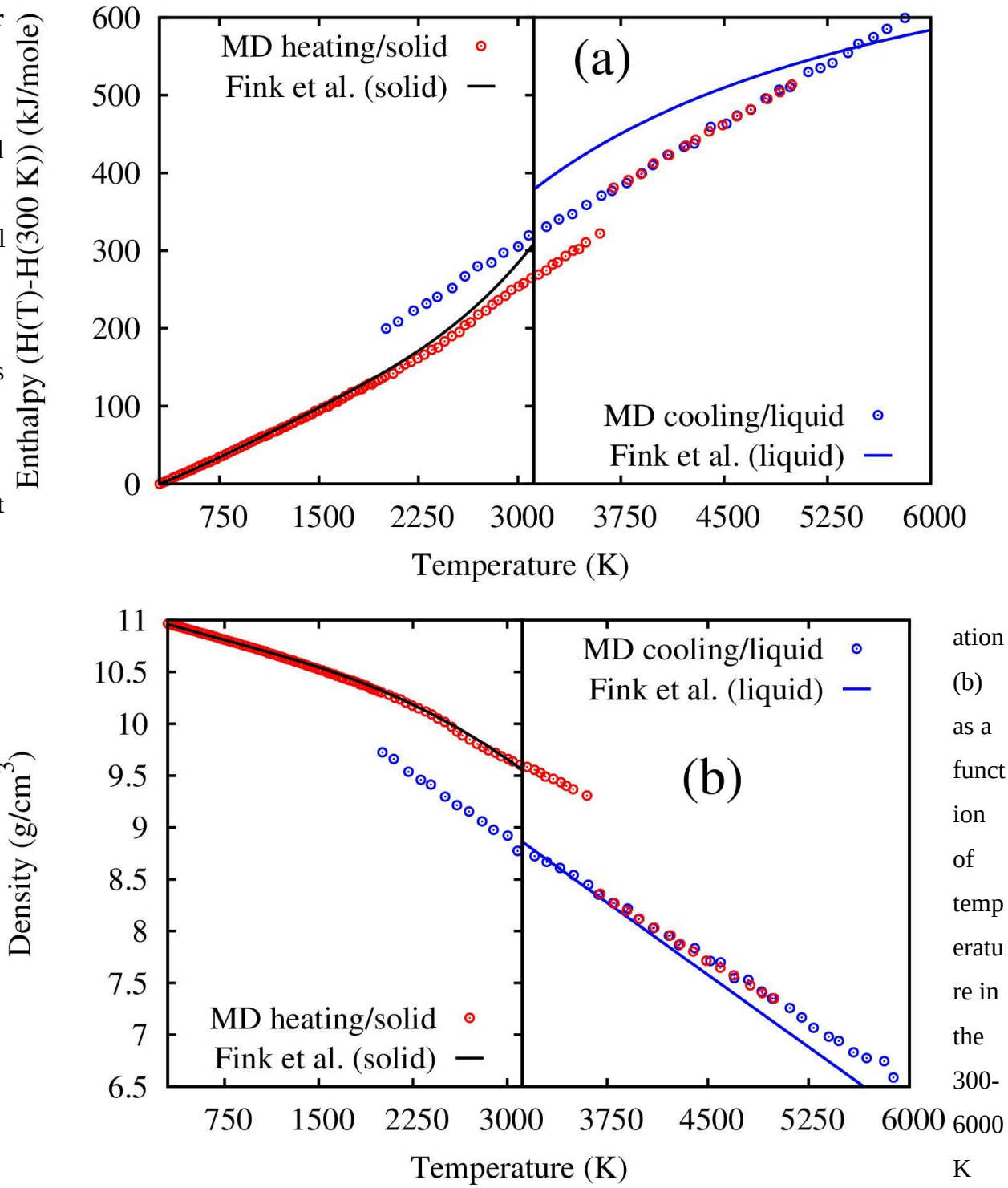

Figure 3: MD calculated enthalpy increments (a) and density variation (b) as a function of temperature in the 300-6000 K range for UO_2 are compared with experimental values reported by Fink *et al.* [28].

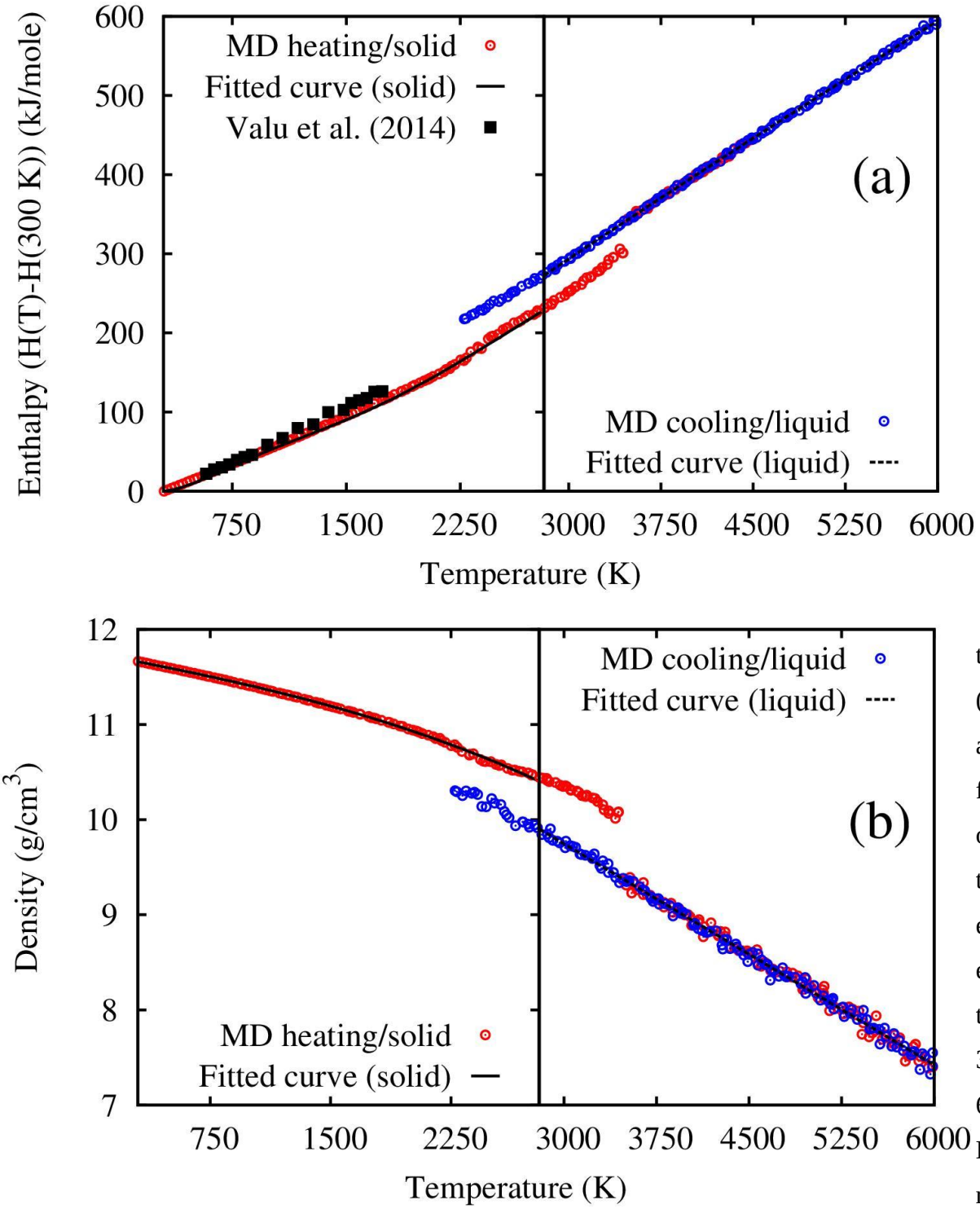

Figure 4: MD calculated enthalpy increments (a) and density variation (b) as a function of temperature in the 300-6000 K range for PuO_2 are compared with experimental values.

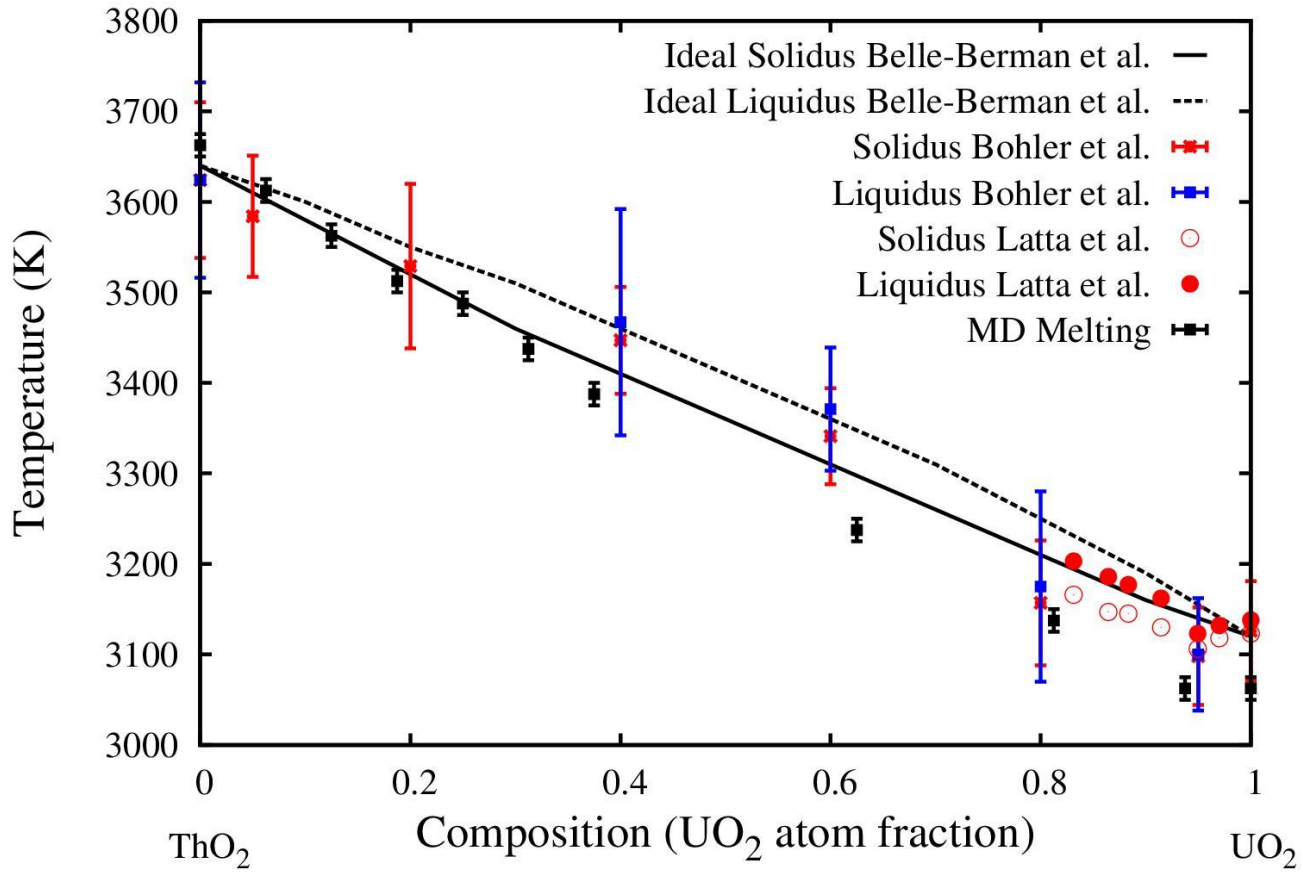

Figure 5: MD calculated melting temperatures of $(Th,U)O_2$ MOX are compared with ideal solidus and liquidus line as well as experimentally reported values.

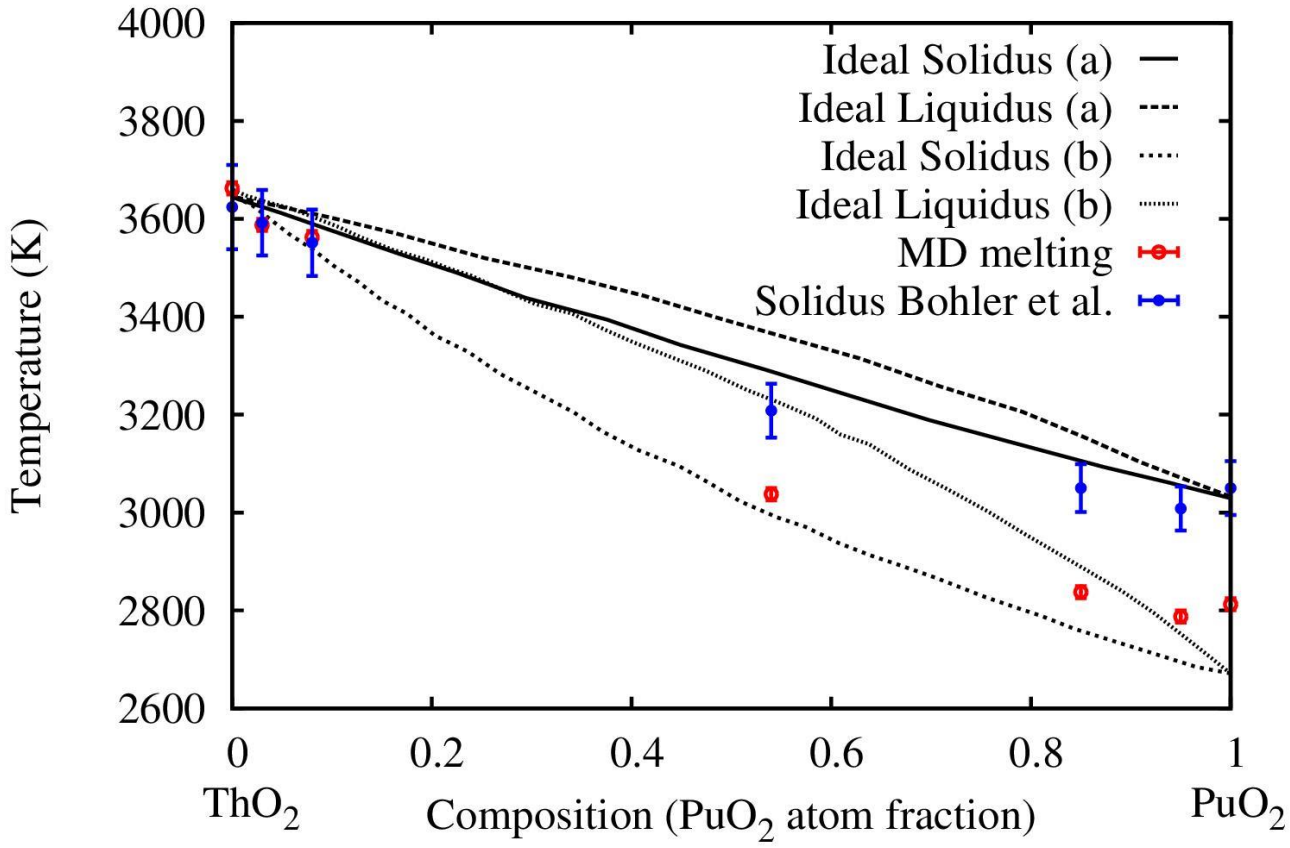

Figure 6: MD calculated melting temperatures of (Th,Pu)O_2 MOX are compared with ideal solidus and liquidus line as well as experimentally reported values by Bohler *et al.* [33]. Ideal behavior represented by (a) and (b) is after Bruycker *et al.* [20] and Bakker *et al.* [46], respectively.

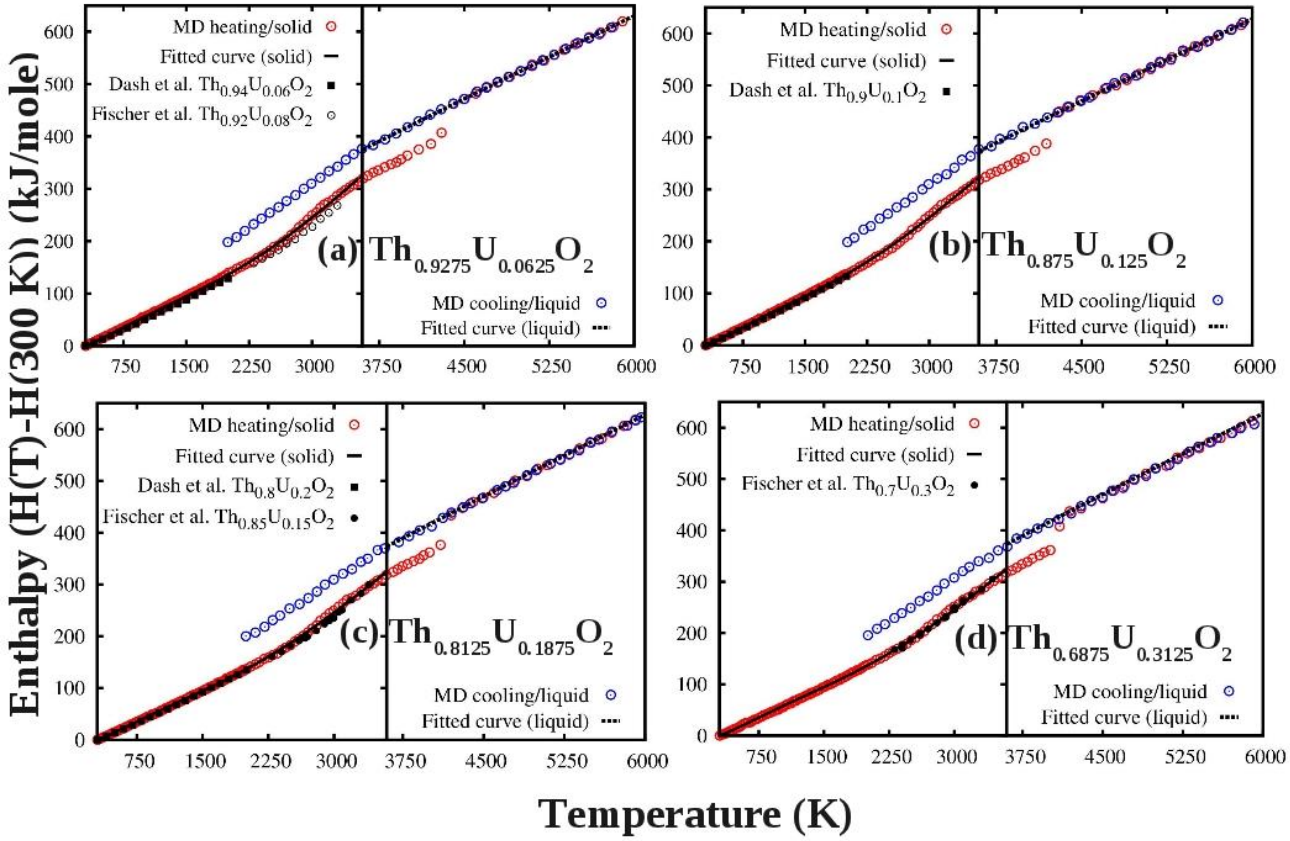

Figure 7: MD calculated enthalpy increments of (a) $Th_{0.9275}Pu_{0.0625}O_2$ (b) $Th_{0.875}Pu_{0.125}O_2$ (c) $Th_{0.8125}Pu_{0.1875}O_2$ (d) $Th_{0.6875}Pu_{0.3125}O_2$ MOX are compared with experimental values reported by Dash *et al.* [24] and Fischer *et al.* [45].

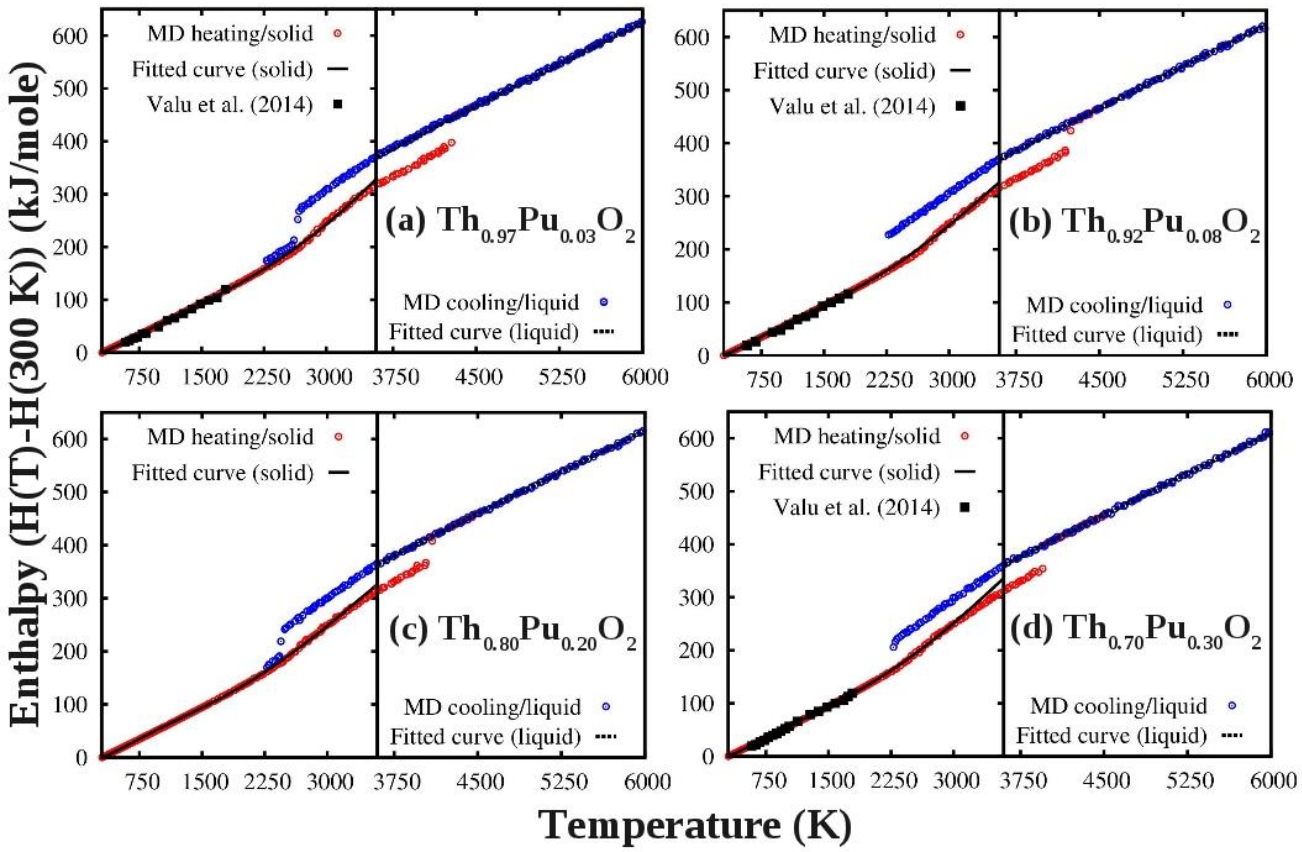

Figure 8: MD calculated enthalpy increments of (a) $Th_{0.97}Pu_{0.03}O_2$ (b) $Th_{0.92}Pu_{0.08}O_2$ (c) $Th_{0.80}Pu_{0.20}O_2$ (d) $Th_{0.70}Pu_{0.30}O_2$ MOX are compared with experimental values reported by Valu *et al.* [34] at the same